Hindawi
International Journal of Photoenergy
Volume 2020, Article ID 7085497, 9 pages
https://doi.org/10.1155/2020/7085497

Research Article

Optical and Thermal Properties of Therminol 55-TiO_2 Nanofluids for Solar Energy Storage

P. Kalidoss, S. Venkatachalapathy, and S. Suresh

Department of Mechanical Engineering, National Institute of Technology, Tiruchirappalli, 620015 Tamil Nadu, India

Correspondence should be addressed to P. Kalidoss; kalidossmech1991@gmail.com

Received 5 November 2019; Revised 10 December 2019; Accepted 6 January 2020; Published 22 January 2020

Guest Editor: Chuanchang Li

The present experimental study focuses on the energy storage performance of Therminol 55-TiO_2 nanofluids for the absorption of solar energy. Photothermal conversion efficiency is enhanced using Fresnel lens and secondary reflectors with a glass-type evacuated absorber tube. The focal length of the Fresnel lens is 150 mm, and that of the secondary reflector is 70 mm. The optical absorbance, extinction coefficient, and thermal conductivity of nanofluids at 100, 250, 350, and 500 ppm are reported. The optical path length of the energy storage medium is 1 cm. The optical performance of the nanofluids is analyzed in the range of 400 to 800 nm. Compared to base fluid, the prepared concentrations show higher absorbance in the measured range of wavelength. The optimum concentration is found to be 250 ppm, and its specific heat is measured in the temperature range of 27 to 117°C and is found to vary from 1.85 to 2.19 J/g°C. The thermal conductivity of the maximum concentration of nanofluid is 0.134 W/mK. The optical absorbance test confirms the stability of nanofluids. Maximum temperature and photothermal conversion efficiency are obtained.

1. Introduction

Liquids are normally used as energy transfer medium for solar thermal collectors. The commonly used liquids are water, silicon oil, Therminol, and mixture of two liquids. The addition of small amounts of nanoparticles to these fluids (low-concentration nanofluids) improves the optical and thermal properties which play a vital role in photothermal conversion. Chen et al. [1] investigated the optical and thermal properties and photothermal conversion of graphene oxide/water-based nanofluids with different mass fractions. They obtained maximum efficiencies of 97.45 and 48.92% at 30 and 80°C for a concentration of 0.02%. The optical absorbance of DI water and ethylene glycol mixture (70 : 30) as base fluid with CuO as a nanoadditive was investigated by Karami et al. [2] for solar applications. Measurements showed that the optical absorbance of nanofluid in the wavelength range of 200 to 2500 nm was 4 times higher than that of the base fluid at 100 ppm concentration. At the same concentration, the enhancement in thermal conductivity was 13.7% at 60°C. The optimum concentration of graphene-water nanofluids was experimentally investigated by Rose et al. [3] in the visible range for solar thermal applications. The volume fraction varied from 0.004 to 0.016%. The maximum absorbance was found at 0.012% with minimum reflectance. The thermal and optical properties of Therminol-Al_2O_3 nanofluid were experimentally investigated by Muraleedharan et al. [4] in the volume concentration ranges from 0.025 to 0.3%. Volume fraction of 0.1% showed maximum absorbance at 501 nm, and the enhancement in thermal conductivity was 11.7%. For the same concentration, the maximum thermal efficiency was 62.7%. To harvest a maximum amount of solar energy, a solar selective volumetric receiver (SSVR) plays an important role as reported by Khullar et al. [5]. In this study, water/MWCNT (multiwalled carbon nanotube) nanofluid was used and its optical transmittance was reported for concentrations of 9, 18, 45, and 75 mg/l. For wavelengths ranging from 300 to 1400 nm, the maximum concentration showed transmittance close to zero indicating maximum absorbance. Wang et al. [6] used paraffin and water-ethanol-based microencapsulated phase change material (MPCM) slurry added with multiwalled carbon nanotubes (MWCNTs) for photothermal conversion. The optical transmittance of the ethanol/water, MWCNT nanofluid (0.005 wt.%), MPCM (1 wt.%), and

hybrid MWCNT-MPCM slurry was reported in the wavelength ranges between 200 and 1400 nm. In the range of wavelength studied, the hybrid nanofluid slurry and MPCM showed 100% absorbance, whereas it was 90% for MWCNT nanofluid in the visible range. The maximum photothermal conversion temperature observed was 80°C after 50 min for MWCNT nanofluid.

The optical properties of MWCNT/water nanofluids of concentration from 0.0015 to 0.25 wt.% were reported by Qu et al. [7]. They measured the optical transmittance in the wavelength range of 200 to 2000 nm. The results revealed that the addition of nanoparticles led to reduction in transmittance. The transmittance was zero for the maximum concentration whereas it was 100% for base fluid up to 900 nm. They also reported a reduction in receiver tube efficiency with increasing time of irradiation. For 0.01 wt.% and an irradiation time of 5 minutes, the receiver tube efficiency was 96.4%. Chen et al. [8] used MWCNT nanofluids with water as base fluid in their studies. They used a concentration of 0.01 wt.% and a temperature range of 10 to 60°C to analyze the stability of pure MWCNT and treated (acid-treated and milling-treated) MWCNT. In the measured range of temperature, the milling treatment showed better stability and higher extinction coefficient (55 mV and 7.49 cm^{-1}, respectively).

Chen et al. [9] studied the thermophysical and optical properties of 0.01, 0.03, and 0.06 wt.% percentage of SiC (silicon carbide) nanofluids with ionic liquid as base fluid. The thermal conductivity and specific heat were also measured. The maximum thermal conductivity for the higher concentration was 0.20 W/mK at 65°C, and the specific heat was 2.5 J/g K at 80°C. The optical properties were studied in the range of 200-1100 nm. The results revealed a transmittance of zero and an extinction coefficient of 7 cm^{-1} for maximum concentration. The optical properties of Al_2O_3 and TiO_2/DI water nanofluids of 0.1 and 0.3% concentration were studied by Said et al. [10]. The extinction coefficient of TiO_2 nanofluid was higher than that of Al_2O_3 nanofluid. The authors found a deviation of nearly 10 times between analytical and experimental results. Khosrojerdi et al. [11] used graphene oxide nanofluid of concentration 0.045 wt.% and thickness of 3 cm in their study and found that 99.6% of incoming solar energy was absorbed. The maximum extinction coefficient was 14 cm^{-1} at 300 nm.

Mahbubul et al. [12] studied the thermal efficiency enhancement of an evacuated tube solar collector using water and CNT/water nanofluids. The thermal conductivity and specific heat of water and 0.05, 0.10, and 0.20 vol.% of nanofluids were measured for the temperatures ranging from 20 to 70°C. For the maximum concentration, the thermal conductivity was 0.9 W/mK at 70°C and the efficiency was 66% which is 10% higher than that of water. The thermal conductivity of Al_2O_3-CuO hybrid nanofluids was reported by Yagnem and Venkatachalapathy [13]. The concentration of nanofluid varied from 0.01 to 0.1%. They obtained a maximum enhancement of 15.72% for 0.1% concentration compared to base fluid. The thermal conductivity of low-concentration nanofluids was investigated by Sundar et al. [14]. They used a mixture of ethylene glycol and water in the proportion of 50 : 50 as base fluid, and the thermal conductivity was measured in the temperature range of 15 to 50°C. For the maximum volume concentration of 0.8%, the enhancement in thermal conductivity was found to vary from 9.8 to 17.89% for Al_2O_3 nanofluid and 15.6 to 24.56% for CuO nanofluid, respectively. The viscosity of water-based single-walled carbon nanohorn (SWCNH) and TiO_2 nanofluids of concentrations 0.001, 0.1, and 1 wt.% was studied by Bobbo et al. [15]. Sodium dodecyl sulphate (SDS) and polyethylene glycol (PEG) were used as stabilizers for SWCNH and TiO_2, respectively. Both the nanofluids showed Newtonian behavior at all concentrations. Zeta potential was reported for all the concentrations, which lies between 57 and 50 mV for SWCNH and 40 and 37 mV for TiO_2 nanofluid. The efficiency was increased by 10% for nanofluid compared to water. Anbu et al. [16] studied heat transfer and pressure drop characteristics of DI water/TiO_2 nanofluids and reported negligible pressure drop for the concentrations 0.1, 0.15, 0.2, and 0.25% compared to base fluid. The heat transfer enhancement was 23 and 4% for tubes with inserts and without inserts for 0.2% volume concentration. Chen et al. [17] reported the absorbance of water-based low-concentration Ag, Au, and Ag-Au nanofluids in the wavelength range of 300 to 800 nm using UV-Spectrophotometer. The concentration used was 0.5 and 2.5 ppm, and a maximum photothermal conversion of 30.97% was obtained for the blended Ag-Au nanofluid. The concentration and thickness of nanofluids play a major role for the maximum absorption of energy radiated by the sun. Thermooptical properties of low-concentration (2.04×10^{-4} and 4.26×10^{-4} volume fraction) gold and silver nanofluids were used by Moreira et al. [18] in their experiments. They obtained an enhancement of 16 and 20% in thermal diffusivity for nanofluids compared to base fluid (DI water). Khullar et al. [19] theoretically studied the thermal efficiency of a concentrated solar parabolic collector using nanofluids. The finite difference method was used for solving the governing equations. Aluminum nanoparticles of concentration 0.05% were used with Therminol VP-1 as base fluid. An evacuated receiver tube was used as the absorber tube. They obtained efficiencies of 19 and 78% for base fluid and nanofluid, respectively, for the average fluid temperature of about 230°C. Tyagi et al. [20] numerically studied heat transfer in a direct absorption solar collector. The authors used water/aluminum nanofluids of volume fraction up to 2%. The collector efficiency depends on its geometry, nanoparticle size, and concentration.

Matuska and Sourek [21] compared the performance of the water heating system using a solar photovoltaic (PV) array (with and without tracking) and a solar photothermal collector. The PV array was connected to the resistive heating elements, and the annual resistance load increase was 20 to 35% for the tracking system. The photothermal conversion efficiency was found to vary between 35 and 68%. The authors concluded that the area required for the photothermal system will be lesser than that for the PV system. The performance of the solar ventilation system coupled with the low-temperature organic Rankine cycle (ORC) was experimentally and numerically investigated by Hung et al. [22]. The dimensions of the system were 4-meter length

and 15° air flow angle. The results of CFD simulations were within the acceptable limit which proved that the CFD is the acceptable tool for predicting the efficiency of the ventilation system. The experimental efficiency of the ORC was 6.2%, and the power generated was 11.43 KWh/day. The optimum concentration for the optical absorbance of Therminol 55-MWCNTs was reported by Kalidoss et al. [23]. The authors concluded that 100 ppm concentration had an absorbance of 0.75 in the visible range and the corresponding photothermal conversion efficiency was 17.36%.

The performance of the solar flat-plate collector was investigated using the reflectors by Bhowmik and Amin [24]. The maximum outlet temperature of water was 52°C for the collector with a reflector. The authors obtained a maximum efficiency of 61% with a reflector which was 10% higher compared to that of a collector without a reflector. Thermal efficiency enhancement of a booster secondary reflector was studied by Bellos and Tzivanidis [25]. They used solid work flow simulation software with syltherm800 as working medium. Turbulent flow was considered in the study, and the authors concluded that the thermal efficiency enhancement varied with an incident angle. The maximum enhancement in efficiency was 150%, and the useful heat gain for the corresponding angle was 10.8 kW. The ray tracking method was used by Prasad et al. [26] to optimize the configuration of the solar Fresnel lens coupled with the secondary reflector system to overcome the improper distribution of heat flux. Optical efficiencies of four different secondary reflectors were reported. The results showed maximum optical efficiency of 75% with a zero-degree tracking error for the compound parabolic concentrator. The minimum optical efficiency was 32% for the trapezoidal secondary concentrator with the tracking error of 0.25 degree.

The major findings on optical absorbance and photothermal conversion efficiency using different nanofluids are given in Table 1.

Many studies have been carried out on the use of low-concentration nanofluids for light to heat conversion. Only few research papers are available with secondary reflectors, and not much work has been done on the combined effects of the above two. The present study focuses on low-concentration nanofluids coupled with secondary reflectors for photothermal conversion.

2. Experiment

2.1. Materials and Characterization. Therminol 55, manufactured by Eastman Chemical Company, USA, is used as base fluid. The chemical name of Therminol 55 is benzene, C14-30-alkyl derivatives, and the molecular formula is $C_{28}H_{50}$. TiO_2 (titanium dioxide) nanoparticles, purchased from Sisco Research Laboratories, India, are used, and the average particle size is 32 nm. The X-ray diffraction (XRD) test is carried out to identify the crystalline structure of TiO_2 nanoparticles, shown in Figure 1. The analysis is carried out in the range of 0-100°, and the peak occurs at 22°. The results reveal that there are no impurities in the nanoparticles.

2.2. Preparation of Nanofluids. Low-concentration nanofluids of 100, 250, 350, and 500 ppm concentrations are prepared by the dilution process shown in Figure 2. 500 ppm is taken as stock solution which is prepared by adding 50 mg of nanoparticles in 100 ml of the base fluid.

The following equation gives the dilution process adopted in this study:

$$C_1 \times V_1 = C_2 \times V_2, \tag{1}$$

where C_1 is the concentration of stock solution prepared (ppm), C_2 is the required concentration of solution to be prepared (ppm), V_1 is the volume of solution required for dilution from stock solution (ml), and $V_2$is the volume of solution to be prepared (ml).

To overcome the agglomeration and also to prevent the settling of nanoparticles, the prepared nanofluid is kept in a magnetic stirrer (REMI make) for 1-hour duration. The nanofluid is then kept in an ultrasonicator (LARK make) for 45 minutes. No surfactant is added to the nanofluid.

2.3. Uncertainty in Measurement. The difference between actual and measured values of the experiments is evaluated, and it is reported as error. The main parameter for photothermal conversion is temperature, which is measured using T-type thermocouples connected to a data logger. To evaluate the error in temperature measurement, the root sum squares (RSS) method is used [27]. The thermocouples are calibrated using a drywell calibrator (Fluke 9100S), and the accuracy of the calibrator is ±0.25°C.

The bias and resolution of the data logger used in this study are ±0.1°C and 0.1°C, respectively. The error in the data logger is found using the following equations.

$$\begin{aligned} e_{\text{DAQ}} &= \sqrt{(e_{\text{bias}})^2 + (e_{\text{precision}})^2}, \\ e_{\text{thermocouple}} &= \sqrt{(e_{\text{bias}})^2 + (e_{\text{precision}})^2}, \\ e_{\text{Temp}} &= \sqrt{\left((e_{\text{thermocouple}})^2 + e_{\text{DAQ}}\right)^2 + (e_{\text{calibrator}})^2}. \end{aligned} \tag{2}$$

The overall uncertainty in temperature measurement is found by combining the errors of the thermocouple, data logger, and drywell calibrator, and the error in temperature is found to be ±1.12°C.

2.4. Description of the Experiment

2.4.1. Experimental Setup. Though nanofluids are used as working medium in the direct solar absorber, their stability plays an important role. To confirm the stability of 250 ppm Therminol-TiO_2 nanofluid, the absorbance test is carried out for every 2 hrs for a duration of 12 hrs using a UV-Vis spectrophotometer. A marginal change in absorbance is observed indicating that there is no precipitation of nanoparticles. The experimental facility consists of secondary reflectors, evacuated tubes, a solar tracker with a time-dependent tracking system, and a Fresnel lens. In order to

Table 1

Author	Base fluid and nanoparticles	Optimum concentration	Optical absorbance (visible range)	Photothermal conversion efficiency	Receiver tube
Chen et al. [1]	Water-graphene oxide	0.02 mass fraction	60% (abs)	48.92%	Cylindrical quartz glass
Karami et al. [2]	Water and ethylene glycol-(70% : 30%) CuO	100 ppm	98% (abs)	—	—
Rose et al. [3]	Ethylene glycol-graphene oxide	0.012 vol. fraction	3 AU	—	—
Muraleedharan et al. [4]	Therminol 55-Al_2O_3	0.1% vol. concentration	1.4 AU	62.7%	Glass-to-glass type (evacuated)
Wang et al. [6]	MPCM slurry/water-ethanol-MWCNTs	0.005 wt.%	100% (abs)	79.8°C (maximum temperature)	Glass-to-glass type (evacuated)
Qu et al. [7].	Water-MWCNTs	0.01 wt.%	100% (abs)	96.4%	Glass tubes
Chen et al. [8]	Water-MWCNTs (milling treated)	0.02 wt.%	100% (abs)	95%	Acrylic receiver
Chen et al. [9]	Ionic liquid-silicon carbide	0.03 wt.%	100% (abs)	—	—
Khosrojerdi et al. [11]	Water-graphene oxide	0.045 wt.%	0.9 AU	—	—
Chen et al. [17]	Water-Ag and Au (hybrid)	2.5 ppm	0.5 AU	30.97%	Glass beakers
Tyagi et al. [19]	Therminol VP-1-Al_2O_3	0.05% vol. concentration	—	78%	Glass-to-glass type (evacuated)
Kalidoss et al. [23]	Therminol 55-MWCNTs	100 ppm	0.75 AU	17.36%	Glass-to-copper type (evacuated)

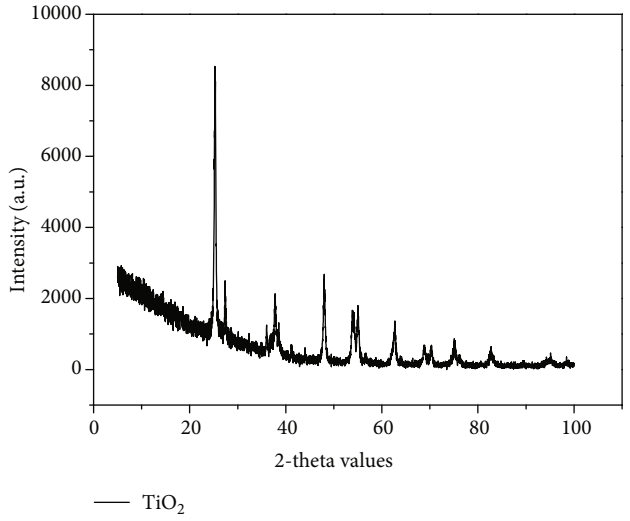

Figure 1: XRD pattern of TiO_2.

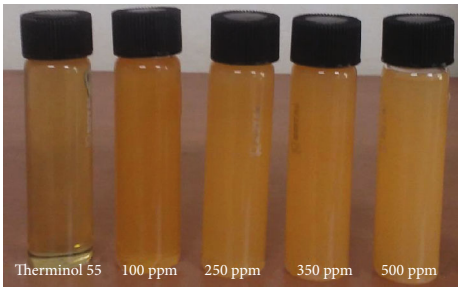

Figure 2: Photographic view of Therminol 55-TiO_2 nanofluids.

fix the secondary reflector at its focal length, a separate arrangement is provided. The schematic diagram of the secondary reflector is shown in Figure 3, and its detailed specifications are given in Table 2. Spacing of 25 mm is given on either side of the Fresnel lens to increase the solar irradiation on the secondary reflectors. Figure 4 shows the top view of the Fresnel lens with spacing.

The photographic view of the experimental setup is depicted in Figure 5. The flow rate of the nanofluid used in the experiment is 0.5 lps, and a rotameter is used to measure the flow rate. The system is supported by an aluminum frame of a rectangular section and the lens side by a square section. The fluid is circulated by a pump, and the circulated fluid is stored in a well-insulated tank. The insulation has a thickness of 40 mm, and its thermal conductivity is 0.03 W/mK. T-type thermocouples are used to measure the temperature of the secondary reflector and nanofluids, and the data are recorded using a Keysight 34972 data logger. The details of the instruments used in the experiment are given in Tables 3 and 4.

The geometrical concentration ratio (CR_g) of the secondary reflector is given by Abdel-Rehim and Lasheen [28].

$$\mathrm{CR_g} = \frac{A_a}{A_r}, \tag{3}$$

$$A_a = L \times d, \tag{4}$$

$$A_r = \frac{2}{3} d \times h, \tag{5}$$

$$h = \frac{d^2}{16f}. \tag{6}$$

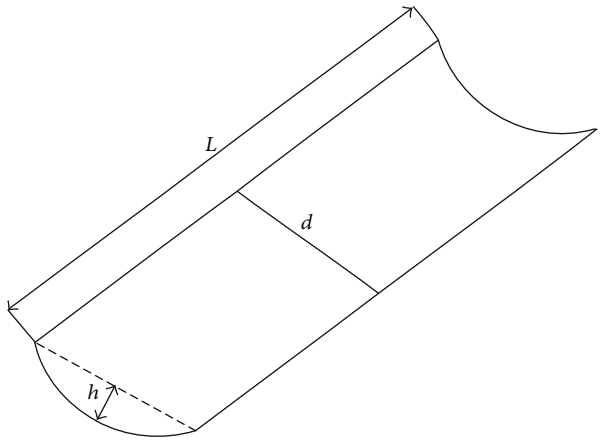

Figure 3: Schematic view of the secondary reflector.

Table 2: Specifications of the secondary reflector.

Parameters	Values
Reflectivity	0.913
Thickness	0.5 mm
Length (L)	550 mm
Width of the receiver (d)	200 mm
Depth (h)	170 mm
Concentration ratio	4.863
Focal length (f)	70 mm

2.4.2. Photothermal Conversion Efficiency. The experiments are carried out during the first 10 days of April 2019. The hourly temperature and the solar insolation are monitored. During the first five days, only the Fresnel lens is used, and for the remaining period, the Fresnel lens is coupled with secondary reflectors and the average values are reported. The recorded temperature values at the specific time are added and divided by the number of days (five days each) for extracting the average values. The same procedure was followed in the research work of Kalidoss et al. [23]. The experimental setup is placed in the surface azimuth angle 0° which is the true north-south direction. A single-axis solar tracking system will track the east-west axis along the movement of the sun. Figure 6 shows the fluid temperature in the storage tank, and the temperature is always higher with secondary reflectors. Maximum temperatures of 110.4 and 93.5°C are obtained at 15:00 p.m. with and without secondary reflectors.

The photothermal conversion efficiency of the Fresnel lens alone and coupled with secondary reflectors is depicted in Figure 7. The efficiency is calculated based on the heat gain by the collector and radiation energy incident on the absorber tubes, given in equation (4). Better photothermal conversion is obtained in both the cases, due to glass-to-glass evacuated tubes which help overcome the convective losses from the absorber tubes. Harding et al. [29] also reported a maximum efficiency of 61.4% for fluid in a glass-to-glass absorber tube compared to other kinds of receiver tubes without secondary reflectors. For the same type of absorber tubes, the maximum efficiency was 62.7% for Therminol 55-Al_2O_3 nanofluid [4].

$$\dot{\eta} = \frac{m_{\mathrm{nf}}\, C_{\mathrm{nf}}}{G\, A}\, \frac{\Delta T}{\Delta t}. \tag{7}$$

The intensity of radiation is measured using a pyranometer. The average values of solar intensity for both the studies are close to 750 W/m^2, shown in Figure 8. The maximum temperature observed for the secondary reflectors is 85°C. The maximum efficiency of the solar collector with and without secondary reflectors is 82.63% at 13:30 p.m. and 61.46% at 13:00 p.m., respectively.

3. Results and Discussion

3.1. Absorbance and Extinction Coefficient. The optical absorbance is measured at a room temperature of 25°C using a Shimadzu UV-2600 spectrophotometer in the wavelength ranging from 400 to 800 nm. Therminol 55 is used as the reference sample throughout the measurement, and a quartz cuvette with path length of 1 cm is used as a sample holder. The spectrophotometer works on the principle of Beer-Lambert's law. According to this law, light absorbed in the sample is directly proportional to the concentration of the sample in which light is radiated. The equation for the absorbance is given as

$$A = \log_{10} \frac{I_{\mathrm{o}}}{I}\, \alpha\, C, \tag{8}$$

where I and I_{o} are the intensities of incident and transmitted light, respectively. The absorbance of the nanofluids with various concentrations is depicted in Figure 9. It is found that the optimum absorbance occurs at 250 ppm concentration in the visible range. The sum of absorption and scattering coefficient is the extinction coefficient and is shown in Figure 10. Though the absorbance and extinction coefficient are higher for 100 ppm concentration, its thermal conductivity is lower. For 350 and 500 ppm, the optical properties are higher in a narrow range and lower in the remaining spectrum in comparison with 250 ppm. Hence, 250 ppm is taken as the optimum concentration for further studies. From absorbance results, transmittance is calculated using the following equation [11]:

$$A = 2 - \log\,(T\%). \tag{9}$$

The extinction coefficient (σ) is calculated by

$$T = \frac{I}{I_{\mathrm{o}}} = \exp^{-L\sigma_{\mathrm{total}}}. \tag{10}$$

The particle size parameter (α) is given by the following equation and is always less than one for solar applications:

$$\alpha = \frac{\pi D}{\lambda}. \tag{11}$$

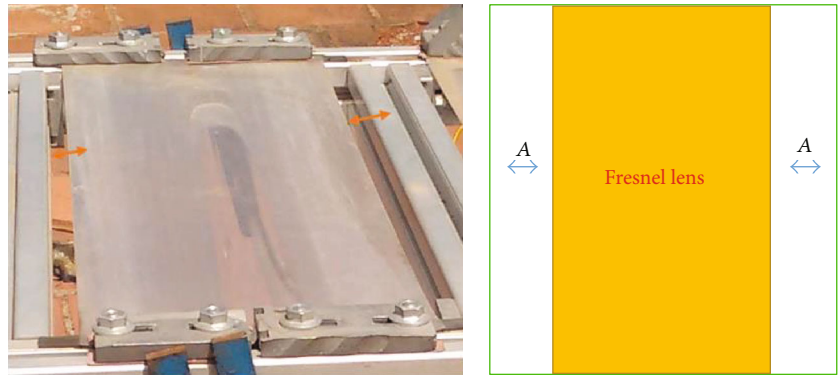

(a) (b)

Figure 4: Top view of the Fresnel lens: (a) photograph and (b) line diagram.

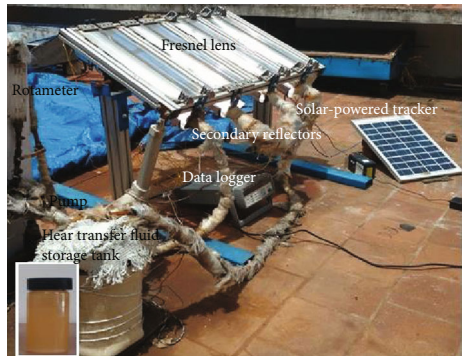

Figure 5: Photographic view of the experimental setup.

Table 3: Specifications of the experimental setup.

Component	Specifications
Fresnel lens	Thickness (250 μm), focal length (150 mm)
Holder (square block)	Aluminum (45 mm)
Absorber tube	Evacuated glass in a glass tube (outer diameter (25 mm), inner diameter (10 mm))
Absorber tube length	550 mm
Thermocouple	T-type

3.2. Thermal Conductivity. The thermal conductivity of Therminol 55-TiO_2 nanofluid is determined using a KD2 Pro Thermal Properties Analyzer (Decagon Devices, Inc., USA). The sensor needle KS-1 is used for measuring the thermal conductivity. The sensor is made of stainless steel, and its dimensions are 60 mm length and 1.3 mm diameter. The sensor needle's measuring range is 0.2-2 W/mK with an accuracy of ±5%. The sensor needle has a heating element and a thermistor. Before starting the measurements, it should be calibrated by standard glycerine solution, prescribed by the manufacturer. The time taken to measure the thermal conductivity of the fluid is 90 seconds, and the instrument requires a 16-bit microcontroller/AD converter. The conductivity is computed from the data in the form of change in temperature and time, given by equation (3).

$$k = \frac{q(\ln t2 - \ln t1)}{4\pi(\Delta T2 - \Delta T1)}. \quad (12)$$

The thermal conductivity of 250 ppm concentration is measured to be 0.129 W/mK. For 350 and 500 ppm, the conductivity values are 0.131 and 0.134 W/mK, respectively.

3.3. Specific Heat. Specific heat of 250 ppm TiO_2 nanofluid is measured with a modulated differential scanning calorimeter (DSC) at IISc, Bangalore. The measurement temperature ranging from 27 to 117°C is shown in Figure 11. The temperature increases at a rate of 10°C/min, and the sample is kept in isothermal condition for 5 min. The TOPEM method is used for finding the specific heat. The sample holder is aluminum whose weight is 49.71 g, and the quantity of the sample used is 29.60 mg. Due to increase in temperature, the specific heat of the nanofluid increases from 1.85 to 2.19 J/g K.

4. Conclusions

The optical and thermal properties of low-concentration Therminol 55-TiO_2 nanofluids are experimentally investigated. The nanofluid concentration varied from 250 to 500 ppm. In the visible range, the absorbance is maximum in a narrow band and remains close to 2.5-3.0 for the remaining wavelength (450-800 nm). Optical stability confirms the suitability of Therminol 55-TiO_2 nanofluid for light to heat conversion in the visible spectrum. The addition of nanoparticles shows changes in thermal conductivity, and an enhancement of 1.57% is found for 250 ppm compared to base fluid. The specific heat measurement shows a marginal change in the temperature range studied. The temperature and photothermal conversion efficiency are enhanced by the use of secondary reflectors, and a maximum efficiency of 82.63% is obtained.

Table 4: Specifications of the instruments used in the experiment.

Instrument	Accuracy
Shimadzu UV-2600 spectrophotometer	±0.1 nm (200 to 1400 nm)
Thermocouples	±0.5°C
Pyranometer	<0.15%
KD2 Pro (thermal conductivity)	±5%
METTLER TOLEDO DSC 1	±0.2°C

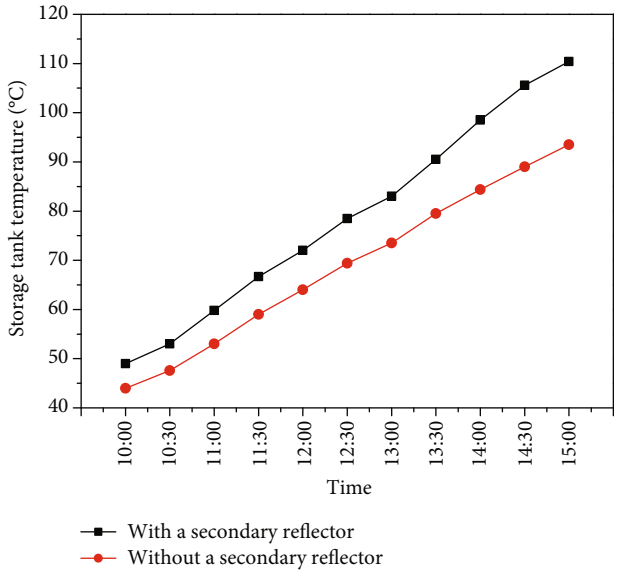

Figure 6: Variation of fluid temperature with time.

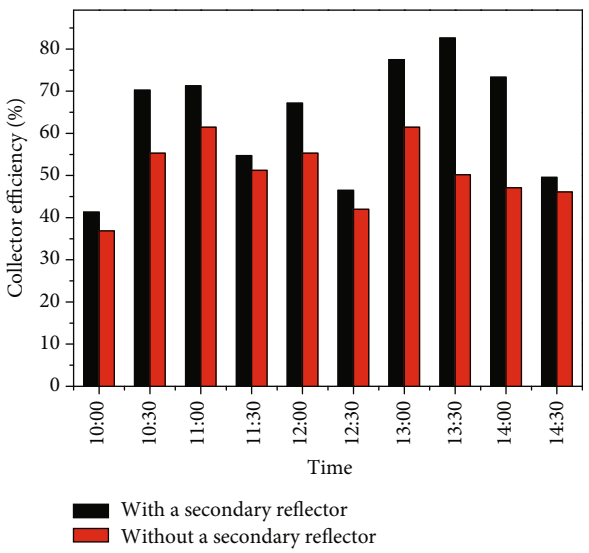

Figure 7: Variation of collector efficiency with time.

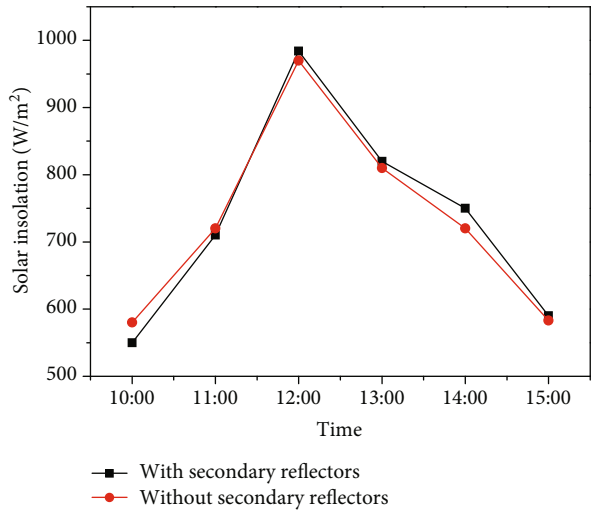

Figure 8: Solar insolation with and without secondary reflectors.

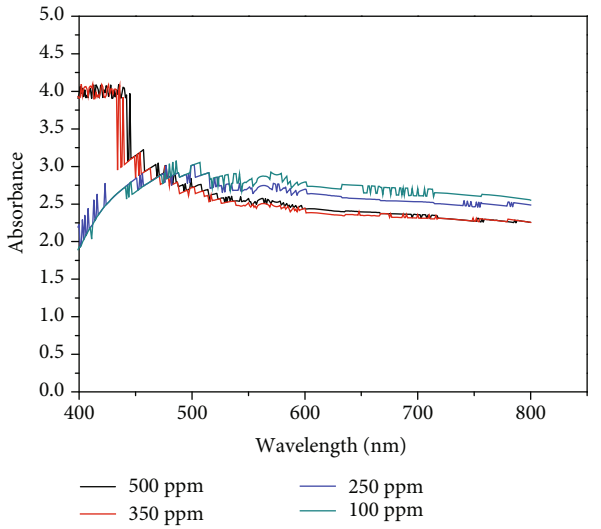

Figure 9: Absorbance of Therminol 55-TiO_2 nanofluids.

Abbreviations

A: Absorbance
A_{total}: Surface area of the receiver tube (m^2)
A_r, A_a: Receiver area and aperture area (m^2)
C: Concentration
C_{nf}: Specific heat of nanofluid (J/g K)
d: Aperture diameter of the secondary reflector (m)
f: Focal length (m)
G: Solar flux on the receiver tube (W/m^2)
h: Depth of the secondary reflector (m)
I_r: Average radiant flux (W/m^2)
I: Intensity of transmitted light
I_o: Intensity of incident light
k: Thermal conductivity (W/m K)
L: Thickness of the sample (cm)
m_{nf}: Mass of nanofluid (kg)
q: Heat flux (W/m^2)

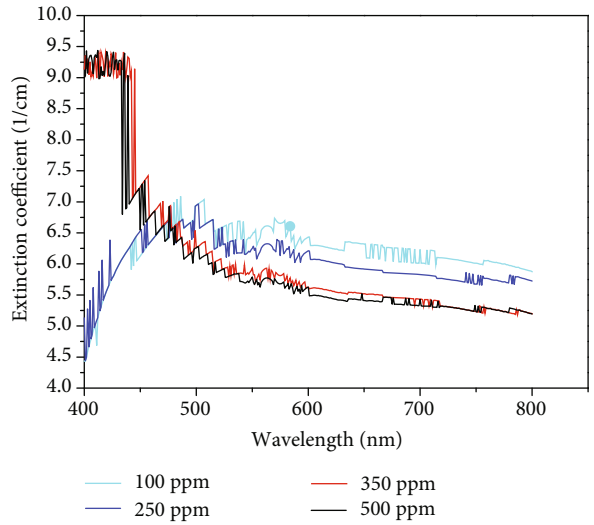

Figure 10: Extinction coefficient of Therminol 55-TiO_2 nanofluids.

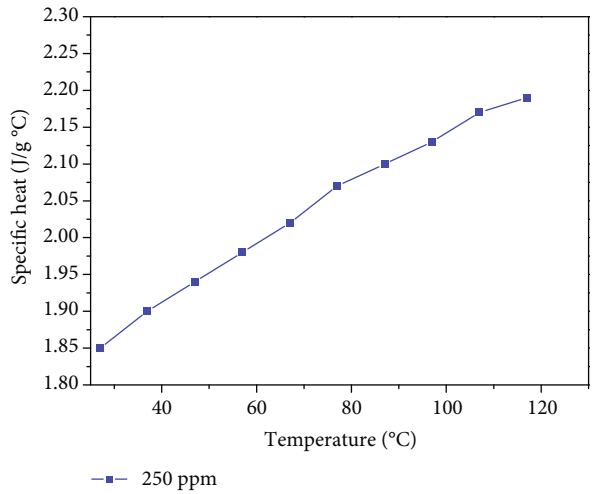

Figure 11: Specific heat variation of 250 ppm Therminol 55-TiO_2 nanofluids.

T: Temperature (K)
t: Time (s)
w: Uncertainty (%)
α: Absorption coefficient
σ: Extinction coefficient (1/cm)
ΔT: Rise in temperature inside the absorber tube (K)
Δt: Exposed time (s).

Data Availability

The data (results) used to support the findings of this study are available from the corresponding author upon request.

Conflicts of Interest

The authors declare that they have no conflicts of interest.

References

[1] L. Chen, C. Xu, J. Liu, X. Fang, and Z. Zhang, "Optical absorption property and photo-thermal conversion performance of graphene oxide/water nanofluids with excellent dispersion stability," *Solar Energy*, vol. 148, pp. 17–24, 2017.

[2] M. Karami, M. A. Akhavan-Behabadi, M. Raisee Dehkordi, and S. Delfani, "Thermo-optical properties of copper oxide nanofluids for direct absorption of solar radiation," *Solar Energy Materials & Solar Cells*, vol. 144, pp. 136–142, 2016.

[3] B. A. J. Rose, H. Singh, N. Verma et al., "Investigations into nanofluids as direct solar radiation collectors," *Solar Energy*, vol. 147, pp. 426–431, 2017.

[4] M. Muraleedharan, H. Singh, S. Suresh, and M. Udayakumar, "Directly absorbing Therminol-Al_2O_3 nano heat transfer fluid for linear solar concentrating collectors," *Solar Energy*, vol. 137, pp. 134–142, 2016.

[5] V. Khullar, H. Tyagi, T. P. Otanicar, Y. L. Hewakuruppu, and R. A. Taylor, "Solar selective volumetric receivers for harnessing solar thermal energy," *Journal of Heat Transfer*, vol. 140, no. 6, 2018.

[6] Z. Wang, J. Qu, R. Zhang, X. Han, and J. Wu, "Photo-thermal performance evaluation on MWCNTs-dispersed microencapsulated PCM slurries for direct absorption solar collectors," *Journal of Energy Storage*, vol. 26, p. 100793, 2019.

[7] J. Qu, M. Tian, X. Han, R. Zhang, and Q. Wang, "Photo-thermal conversion characteristics of MWCNT-H_2O nanofluids for direct solar thermal energy absorption applications," *Applied Thermal Engineering*, vol. 124, pp. 486–493, 2017.

[8] W. Chen, C. Zou, and X. Li, "Application of large-scale prepared MWCNTs nanofluids in solar energy system as volumetric solar absorber," *Solar Energy Materials and Solar Cells*, vol. 200, no. 8, p. 109931, 2019.

[9] W. Chen, C. Zou, and X. Li, "An investigation into the thermophysical and optical properties of SiC/ionic liquid nanofluid for direct absorption solar collector," *Solar Energy Materials and Solar Cells*, vol. 163, pp. 157–163, 2017.

[10] Z. Said, R. Saidur, and N. A. Rahim, "Optical properties of metal oxides based nanofluids," *International Communications in Heat and Mass Transfer*, vol. 59, pp. 46–54, 2014.

[11] S. Khosrojerdi, A. M. Lavasani, and M. Vakili, "Experimental study of photothermal specifications and stability of graphene oxide nanoplatelets nanofluid as working fluid for low-temperature direct absorption solar collectors (DASCs)," *Solar Energy Materials and Solar Cells*, vol. 164, pp. 32–39, 2017.

[12] I. M. Mahbubul, M. M. A. Khan, N. I. Ibrahim, H. M. Ali, F. A. Al-Sulaiman, and R. J. R. E. Saidur, "Carbon nanotube nanofluid in enhancing the efficiency of evacuated tube solar collector," *Renewable Energy*, vol. 121, pp. 36–44, 2018.

[13] A. R. Yagnem and S. Venkatachalapathy, "Heat transfer enhancement studies in pool boiling using hybrid nanofluids," *Thermochimica Acta*, vol. 672, pp. 93–100, 2019.

[14] L. S. Sundar, M. H. Farooky, S. N. Sarada, and M. K. Singh, "Experimental thermal conductivity of ethylene glycol and water mixture based low volume concentration of Al_2O_3 and CuO nanofluids," *International Communications in Heat and Mass Transfer*, vol. 41, pp. 41–46, 2013.

[15] S. Bobbo, L. Fedele, A. Benetti et al., "Viscosity of water based SWCNH and TiO_2 nanofluids," *Experimental Thermal and Fluid Science*, vol. 36, pp. 65–71, 2012.

[16] S. Anbu, S. Venkatachalapathy, and S. Suresh, "Heat transfer and pressure drop studies of TiO 2/DI water nanofluids in helically corrugated tubes using spiraled rod inserts," *Heat and Mass Transfer*, vol. 54, no. 5, pp. 1301–1311, 2018.

[17] M. Chen, Y. He, J. Huang, and J. Zhu, "Synthesis and solar photo-thermal conversion of Au, Ag, and Au-Ag blended plasmonic nanoparticles," *Energy Conversion and Management*, vol. 127, pp. 293–300, 2016.

[18] L. M. Moreira, E. A. Carvalho, M. J. V. Bell et al., "Thermo-optical properties of silver and gold nanofluids," *Journal of Thermal Analysis and Calorimetry*, vol. 114, no. 2, pp. 557–564, 2013.

[19] V. Khullar, H. Tyagi, P. E. Phelan, T. P. Otanicar, H. Singh, and R. A. Taylor, "Solar energy harvesting using nanofluids-based concentrating solar collector," *Journal of Nanotechnology in Engineering and Medicine*, vol. 3, no. 3, 2012.

[20] H. Tyagi, P. Phelan, and R. Prasher, "Predicted efficiency of a low-temperature nanofluid-based direct absorption solar collector," *Journal of Solar Energy Engineering*, vol. 131, no. 4, 2009.

[21] T. Matuska and B. Sourek, "Performance analysis of photovoltaic water heating system," *International Journal of Photoenergy*, vol. 2017, 10 pages, 2017.

[22] T.-C. Hung, D.-S. Lee, and J.-R. Lin, "An innovative application of a solar storage wall combined with the low-temperature organic Rankine cycle," *International Journal of Photoenergy*, vol. 2014, 12 pages, 2014.

[23] P. Kalidoss, S. Venkatachalapathy, and S. Suresh, "Photothermal energy conversion enhancement studies using low concentration nanofluids," *Journal of Solar Energy Engineering*, vol. 141, no. 6, 2019.

[24] H. Bhowmik and R. Amin, "Efficiency improvement of flat plate solar collector using reflector," *Energy Reports*, vol. 3, pp. 119–123, 2017.

[25] E. Bellos and C. Tzivanidis, "Investigation of a booster secondary reflector for a parabolic trough solar collector," *Solar Energy*, vol. 179, pp. 174–185, 2019.

[26] G. S. C. Prasad, K. S. Reddy, and T. Sundararajan, "Optimization of solar linear Fresnel reflector system with secondary concentrator for uniform flux distribution over absorber tube," *Solar Energy*, vol. 150, pp. 1–12, 2017.

[27] B. Praveen and S. Suresh, "Experimental study on heat transfer performance of neopentyl glycol/CuO composite solid-solid PCM in TES based heat sink," *Engineering Science and Technology, an International Journal*, vol. 21, no. 5, pp. 1086–1094, 2018.

[28] Z. S. Abdel-Rehim and A. Lasheen, "Experimental and theoretical study of a solar desalination system located in Cairo, Egypt," *Desalination*, vol. 217, no. 1-3, pp. 52–64, 2007.

[29] G. L. Harding, Y. Zhiqiang, and D. W. Mackey, "Heat extraction efficiency of a concentric glass tubular evacuated collector," *Solar Energy*, vol. 35, no. 1, pp. 71–79, 1985.